Electric Power Systems Research 80 (2010) 1277–1285

Contents lists available at ScienceDirect

Electric Power Systems Research

journal homepage: www.elsevier.com/locate/epsr

Demagnetization diagnosis in permanent magnet synchronous motors under non-stationary speed conditions

Jordi-Roger Riba Ruiz [a,*], Antonio Garcia Espinosa [b,1], Luís Romeral [c,2], Jordi Cusidó [c]

[a] EUETII, Dept. d'Enginyeria Elèctrica, Universitat Politècnica de Catalunya, Plaça del Rei 15, 08700 Igualada, Barcelona, Spain
[b] Dept. d'Enginyeria Elèctrica, Universitat Politècnica de Catalunya C/Colom 1, 08222 Terrassa, Spain
[c] Dept. d'Enginyeria Electrònica, Universitat Politècnica de Catalunya C/Colom 1, 08222 Terrassa, Spain

ARTICLE INFO

Article history:
Received 27 December 2008
Received in revised form 21 April 2010
Accepted 29 April 2010
Available online 23 May 2010

Keywords:
Time–frequency transforms
Hilbert Huang
PMSM
Fault detection
Fault diagnosis

ABSTRACT

Permanent magnet synchronous motors (PMSMs) are applied in high performance positioning and variable speed applications because of their enhanced features with respect to other AC motor types. Fault detection and diagnosis of electrical motors for critical applications is an active field of research. However, much research remains to be done in the field of PMSM demagnetization faults, especially when running under non-stationary conditions. This paper presents a time–frequency method specifically focused to detect and diagnose demagnetization faults in PMSMs running under non-stationary speed conditions, based on the Hilbert Huang transform. The effectiveness of the proposed method is proven by means of experimental results.

1. Introduction

Industry constantly demands products that are faster and more reliable. In this context, for some critical applications, permanent magnet synchronous motors (PMSMs) possess characteristics superior to induction motors. PMSMs are becoming widely applied in high performance positioning and variable speed applications because of their attractive features. Powerful rare earth magnet materials that are now cost-effective, such as Sm–Co and Nd–Fe–B, greatly enhance their properties. PMSMs possess a higher power density than induction motors with equivalent ratings. Advantages of PMSMs include high-speed operation, precise torque control, compactness, high power to weight ratio and high efficiency. Every day they are gaining ground in the automotive, robotics and aeronautical industries [1]. Additional applications of PMSM include gearless elevators in low- and high-rise buildings, centrifugation equipment, as well as the medical, chemical and semiconductor industries, among others.

Many of the applications where PMSMs are applied are critical, as their faults could potentially cause plant shutdown, huge economic loss and even human casualties. Hence, fault detection and diagnosis is one of the most serious areas of concern in the electric drives research field. Therefore, accurate diagnosis of incipient faults in critical applications where PMSMs play an important role can significantly improve system availability and reliability.

A new trend and challenge in the electric drives industry is the design of fault tolerant control systems which provide control algorithms capable of maintaining stability and performance of the controlled system despite the occurrence of faults. To meet this objective, fault detection and diagnosis of electric drives has become an essential tool in most fault tolerant control system designs.

In order to measure the impact of faults, the transient process of the machine under fault conditions must be studied, since this state usually reflects the worst case scenario that the machine designers may face [2]. While there is already a plethora of literature on the study of induction motors, it nevertheless continues to be a dynamic field of investigation [3–7]. Recently, Gritli et al. [8] conducted an interesting study to detect rotor faults on doubly fed induction machines due to unbalanced rotor phase windings. In this study Gritli et al. take advantage of the multiresolution analysis capabilities of the discrete wavelet transform when the machine operates under load-varying conditions and apply a multiresolution fault indicator based on the mean power at different resolution levels to perform a quantitative evaluation of the fault degree.

Conversely, in the case of permanent magnet synchronous motors – whether dc or ac brushless – both drive control and fault detection are relatively novel fields of investigation [1,9–13].

* Corresponding author. Tel.: +34 938035300; fax: +34 938031589.
E-mail addresses: jordi@euetii.upc.edu (J.-R.R. Ruiz), garciae@ee.upc.edu (A. Garcia Espinosa), romeral@eel.upc.edu (L. Romeral), jcusido@eel.upc.edu (J. Cusidó).
[1] Tel.: +34 937398155.
[2] Tel.: +34 937398510.

0378-7796/$ – see front matter © 2010 Elsevier B.V. All rights reserved.
doi:10.1016/j.epsr.2010.04.010

This work presents a innovative method in order to diagnose the demagnetization fault in PMSMs. This fault can be due to an over current on the stator windings that creates a magnetic flux opposed to the natural flux of the magnet and leads to a demagnetization of the magnet. However, the major difficulty with PMSMs occurs at high speed when the induced eddy currents cause heating in the magnet. As the demagnetization curve of the material is highly temperature-dependent, heating effects may induce changes in magnetic properties of the material. In any case, the demagnetization of the permanent magnet results in a reduction of the torque production, generating torque pulsation, vibrations and excessive heat. Other faults that can occur in the motor are shorted turns, open turns, eccentricity and damaged bearings.

Different fault detection and diagnose methods have been applied to detect motor faults, the most common of which are motor current signature analysis (MCSA), vibration analysis and axial flux. Among them MCSA is one of the most popular as it is a non-invasive method, needing only to acquire the line currents of the motor and then to perform the fast Fourier transform (FFT).

It is well known that when the FFT is performed in a PMSM with a faulty rotor, different harmonics appear in the spectrum. They can be identified as [14–16],

$$f_f = f_e \left(1 \pm \frac{k}{P}\right) \tag{1}$$

where f_f is the fault frequency, f_e is the electrical fundamental frequency, k is an integer and P is the number of pole pairs.

In the study carried out in this work, healthy and faulty PMSMs with three pairs of poles are analyzed. The faulty motors studied have just one rotor pair of poles which are partially demagnetized. In this particular case, Eq. (1) can be rewritten as

$$f_f = f_e \left(1 \pm \frac{2k+1}{P}\right) \tag{2}$$

being $k = 0,1,2,\ldots$ an integer.

Taking into account the number of pole pairs of the analyzed motors, in one electrical fundamental period 1/3 of a complete rotation of the rotor is produced. Thus, due to the damaged magnets, there is a pronounced change in the flux density curve around the rotor [15]. This results in an electrical frequency component at the rotating frequency of the rotor, that is, the odd harmonics such as 1/3 and 5/3 among others.

In case of non-stationary motor speed, faulty frequencies are not fixed and fault detection is not evident when using standard FFT. In this paper, a novel method for demagnetization fault detection of PMSMs under non-stationary speed conditions is presented, based on stator current signal decomposition using the Hilbert Huang transform (HHT).

This paper is divided into four sections. Following the introduction, Section 2 presents and discusses signal-processing methods for transient analysis. Section 3 introduces HHT and corresponding algorithms to obtain the time–frequency representation of a non-stationary signal. Experimental results are presented in Section 4, as well as feature extraction by means of energy content of the signal. Finally, conclusions are stated in Section 5.

2. Analysis methods for fault detection

Most of the signals obtained from natural phenomena and from measurements in industrial applications are of a transient nature. Therefore, these types of signals are essentially nonlinear and non-stationary, and traditional signal analysis methods such as Fourier transform fails when dealing with them [17]. Among them, the most likely applied method in industrial environments is based on the Fourier analysis of the steady-state stator currents and the study of the harmonic components that appear around the fundamental component. Fourier analysis of stator currents provides robust results when the machine operates under a certain load level and stationary regime, but has important drawbacks when applied to diagnose the condition of light-loaded machines or machines running under non-stationary load conditions [18].

The Fourier transform is not well suited for analyzing non-stationary signals since it projects the signal on infinite sinusoids which are completely delocalized in time. In dealing with non-stationary signals this is a very important drawback as it is essential to take into account both time and frequency variables. Consequently, a time–frequency representation (TFR) is needed. TFR can be understood as a two-dimensional view of a time-dependent signal represented over both time and frequency axes.

Several time–frequency analysis methods (some of them based on Fourier analysis) have been developed, although successful application of these techniques require a thorough understanding of their respective limitations. For example, the short-time Fourier transform (STFT) allows time–frequency analysis using the widely applied fast Fourier transform (FFT) algorithm. STFT implicitly assumes the signal behaves as stationary during the window interval of computation. The selection of a suitable window size is required to match with the specific frequency content of the signal, which is generally not known *a priori*. This provokes an inconsistent treatment at different frequencies due to the fixed length of the window. Therefore, its application for fault detection is limited to signals where frequency content changes very slowly over time.

Another widely applied time–frequency method is the wavelet transform (WT) which overcomes some of the limitations related to the STFT. WT allows decomposing the raw signal by means of a set of wavelets (basis functions) which are localized both in time and frequency [19]. However, WT presents a serious drawback due to the necessity of *a priori* knowledge about the kind of scale elements which are present in the signal for isolating and analyzing them. As pointed out by Antonino-Daviu et al. [18,20] the selection of the mother wavelet is somewhat arbitrary, since there is no clear rule for selecting the optimal mother wavelet for a specific application. Furthermore, the possible overlap between frequency bands associated with the wavelet signals or the dyadic frequency decomposition of the Mallat algorithm (especially when dealing with the discrete wavelet transform) can result in a limited resolution of some frequency components closer to the fundamental. Another drawback related with this method is the boundary distortion introduced by the WT that in some cases might make the identification of some frequency components difficult.

Some of the drawbacks related to the FT and the WT can be overcome by applying the HHT. HHT possesses advantages over WT because it avoids the selection of the mother wavelet. It also allows for a more valuable study of some frequency components closer to the fundamental as it does not perform the dyadic frequency decomposition of the Mallat algorithm.

3. Hilbert Huang transform

The HHT was proposed by Huang et al. [21] and it has been successfully applied in diverse areas such as geosciences and remote sensing applications [17], nonlinear structural dynamics [22], analysis of sea waves [23], analysis of electroencephalogram (EEG) signals [24], gear fault diagnosis [25], analysis of torsional shaft oscillations [26], analysis of electrical generator coherency [27] and detection of broken rotor bars in induction machines [18], among others.

However, as pointed out by Antonino-Daviu et al. [20] the patterns arising from the HHT appear less clear when compared with the DWT approaches. Furthermore, constraints such as the boundary distortion are not completely avoided. HHT performs the empirical mode decomposition (EMD) of the raw signal. This pro-

cedure allows extracting some components with zero mean from a non-stationary signal, called intrinsic mode functions (IMFs), which are related to characteristic frequency bands of the original signal. IMFs allow the spectral composition of the original signal to be analyzed. Once the EMD has been performed, the Hilbert transform of the IMFs is realized in order to study the instantaneous frequencies of the original signal, allowing a detailed time–frequency analysis of the non-stationary original signal to be carried out.

The Hilbert transform (HT) allows computing a time–frequency distribution from a non-stationary narrow band signal. This is a very limiting drawback of this method [28] because this condition is not normally satisfied by non-stationary signals of interest in practical applications. Huang et al. [21] proposed the application of the EMD to overcome this difficulty. The Hilbert transform can be applied to the IMFs arising from the EMD because each one contains a narrow band component of the signal at a given time.

3.1. Empirical mode decomposition (EMD)

In this section the procedure to perform the empirical mode decomposition is detailed. The EMD of a measured signal $x(t)$ extracts its intrinsic oscillations through their characteristic time scales [29]. The IMFs are extracted by means of an iterative process. Note that the original signal $x(t)$ can be designated as a time series. The procedure usually applied to extract the IMFs of the measured signal can be summarized as follows [27,29]:

1. Extraction of local maxima and minima of the signal $x(t)$. Connect local maxima by applying preferably cubic spline interpolation [30]. Huang et al. [21] have shown that more complex fitting functions marginally improves the resolution while significantly increasing the computational burden. Hence, the upper envelope $e_u(t)$ is generated. Similarly, the lower envelope $e_l(t)$ is generated by connecting local minima by means of cubic spline interpolation.
2. Compute the mean envelope from upper and lower envelopes as,
$$e_m(t) = 0.5[e_u(t) + e_l(t)] \tag{3}$$
3. Obtain the difference series $d(t)$, calculated as the difference between the original series and the mean envelope as,
$$d(t) = x(t) - e_m(t) \tag{4}$$
4. The difference series $d(t)$ might be the first IMF if it meets two requirements. Firstly, the number of local extremes of $d(t)$ and the number of zero crossings must differ at most by one. Secondly, the mean value of $d(t)$ must be close to zero according to some well-established stopping criterion in order to keep the resulting IMFs to be physically meaningful. Detailed information about stopping criterion can be found in [28]. If $d(t)$ is not an IMF, then replace $x(t)$ by $d(t)$ and repeat steps 1–4 until the new $d(t)$ satisfies the conditions of being an IMF. In this case $IMF_1 = d(t)$.
5. Compute the residue $r_1(t)$ as,
$$r_1(t) = x(t) - IMF_1(t) \tag{5}$$
6. Successive IMFs are extracted with an iterative process. They are designed as IMF_i, being $i = 1, 2, \ldots, n$ the number of IMFs of the decomposition. For this purpose, the new signal can be replaced by the residue $r_1(t)$, and steps 1–5 of the process are repeated to extract the rest of the IMFs inherent to the original signal $x(t)$ as,
$$\begin{cases} x(t) = IMF_1(t) + r_1(t) \\ r_1(t) = IMF_2(t) + r_2(t) \\ \quad\quad \cdots \\ r_{n-1}(t) = IMF_n(t) + r_n(t) \end{cases} \tag{6}$$

The signal decomposition process is completed when $r_n(t)$ becomes a monotonic function, from which no further IMFs can be extracted [31].

Finally, it is easily deducible that by applying Eq. (6) the original measured signal $x(t)$ can be reconstructed as:

$$x(t) = \sum_{i=1}^{n} IMF_i(t) + r_n(t) \tag{7}$$

$r_n(t)$ being the residue resulting from the empirical mode decomposition.

The IMF extraction process guarantees that they are obtained in decreasing order of their local frequency content. This means that the first IMF to be obtained contains the modes with highest local frequency content [27]. EMD allows an effective construction of the frequency spectrum of a non-stationary signal containing multiple frequency components. As described in Eq. (7), EMD separates a signal into several IMFs and a residual, all of which can be used for extracting spectral information as well as filtering the signal. As each IMF contains a specific interval of frequencies, they can also be used to perform a digital filtering of the sampled signal $x(t)$.

The IMFs arising from the EMD of the original signal $x(t)$ have narrow band frequency content. Therefore, the Hilbert transform can be applied to the IMFs. From the output of the Hilbert transform the instantaneous frequency and energy contained in the IMFs at each instant of time are computed and a time–frequency matrix is generated which can be represented as a contour plot.

3.2. Hilbert transform (HT)

When dealing in the time domain, the Hilbert transform $y(t)$ of a non-stationary and narrow band signal $x(t)$ can be defined as a convolution between the Hilbert transformer $1/(\pi t)$ and the signal $x(t)$ [32],

$$y(t) = H[x(t)] = \frac{1}{\pi} P \int_{-\infty}^{+\infty} \frac{x(\tau)}{t-\tau} d\tau \tag{8}$$

P being the Cauchy principal value.

The improper integral defined in Eq. (8) frequently does not exist due to the pole placed at $t = \tau$. The Cauchy principal value P allows expanding the type of functions for which the integral exists [33]. Let $x(t)$ be a function defined on $[a,b]$. If $x(t)$ is unbounded near a point ζ of $[a,b]$, the integral of $x(t)$ over $[a,b]$ does not always exist. However, the two limits of Eq. (9) still may exist.

$$\lim_{\epsilon \to 0} \int_a^{\xi - \epsilon} x(t)dt, \quad \lim_{\epsilon \to 0} \int_{\xi + \epsilon}^{b} x(t)dt \tag{9}$$

If the sum of the two above limits exists, the result is the principal value integral of $x(t)$ over $[a,b]$ and is denoted by,

$$P \int_a^b x(t)dt = \lim_{\epsilon \to 0^+} \int_a^{\xi - \epsilon} x(t)dt + \lim_{\epsilon \to 0^+} \int_{\xi + \epsilon}^{b} x(t)dt \tag{10}$$

An analytic signal $z(t)$ is defined as [21,18,31],

$$z(t) = x(t) + iH[x(t)] = x(t) + iy(t) \tag{11}$$

i being the imaginary unit. Eq. (11) can be rewritten in polar form as,

$$z(t) = x(t) + iH[x(t)] = M(t)e^{i\theta(t)} \tag{12}$$

From the phase angle of the polar form, the instantaneous frequency of the analytical signal is then calculated as,

$$\omega(t) = \frac{d\theta(t)}{dt} \tag{13}$$

Accordingly, the real part of the signal $x(t)$ can be written in terms of the amplitude and instantaneous frequency as a time-dependent function,

$$x(t) = \text{Real}(z(t)) = \text{Real}\left(M(t)e^{i\int \omega(t)dt}\right) \tag{14}$$

By combining Eqs. (7) and (14) the result is,

$$x(t) = \text{Real}\left(\sum_{i=1}^{n} M_{IMF,i}(t)e^{i\int \omega_{IMF,i}(t)dt}\right) \tag{15}$$

being [21],

$$\begin{cases} M_{IMF,i}(t) = \sqrt{IMF_i^2(t) + H[IMF_i^2(t)]} \\ \omega_{IMF,i}(t) = \dfrac{d\theta_{IMF,i}(t)}{dt} = \dfrac{d}{dt}\left[\tan^1\left(\dfrac{H[IMF_i(t)]}{IMF_i(t)}\right)\right] \end{cases} \tag{16}$$

In Eq. (15) the term r_n has been omitted since it is a monotonic function and does not contain information about the frequency content of the signal.

The Fourier series representation of a signal $x(t)$ is given by the next equation,

$$x(t) = \text{Real}\left(\sum_{i=1}^{n} M_{Fou,i}e^{i\omega_{Fou,i}(t)t}\right) \tag{17}$$

$M_{Fou,i}$ and $\omega_{Fou,i}$ both being constants. Conversely, both coefficients $M_{IMF,i}$ and $\omega_{IMF,i}$ arising from Eq. (15) are time-dependent. In comparing (15) and (17) it is easy to deduce that (15) can be understood as a generalized Fourier expansion. As shown in Eq. (16), the HT of the IMFs allows the amplitude and the frequency components to be separated. Performing the EMD previous to the HT enables the generation of a variable amplitude and frequency representation, overcoming the limitations imposed by the Fourier analysis, specifically, the independence of amplitude and frequency with respect to time. Thus, the EMD process followed by the Hilbert transform enables time–frequency representation of a non-stationary signal by computing its time-dependent amplitude and the characteristic frequency components at different time instants. This time–frequency representation of a non-stationary signal $x(t)$ is known as the Hilbert Huang spectrum.

4. Experimental results

In this section experimental results are presented. A PMSM with 3 pairs of poles manufactured by ABB, rated torque of 2.3 Nm, 230 VAC and rated speed of 6000 rpm was used in experiments. The motor was driven by an ABB power converter model DGV 700. The drive control was a vector control, with a set point $i_d = 0$ and a PID speed control loop. The motor was loaded by an additional PMSM driven by a torque controller as shown in Fig. 1. A constant load was imposed during experiments.

Demagnetization of the motor was carried out during manufacture. A special motor with reduced magnetization was ordered to perform this task, with 50% of nominal flux in one pair of poles. Nominal flux density is 0.85 T and remanent flux density B_r is 1.19 T.

Experiments were carried out with healthy and faulty motors running under dynamic speed conditions (speed changes from 6000 to 5500 and 3000 to 2500 rpm were induced, see Fig. 2) and under rated load and one-half load.

Stator currents of the PMSM were measured with a Tektronix AC/DC current probe model A622. Motor currents were sampled during approximately 0.26 s at a rate of 6 kHz, obtaining 1601 samples. Data acquisition is done with a DAQ NI PCI-6251 multifunction board, with 16 input channels, 16 bits of resolution and 4k samples of inner memory. The HHT-related algorithms have been implemented in Matlab using the toolbox for Matlab programmed by Rilling [34].

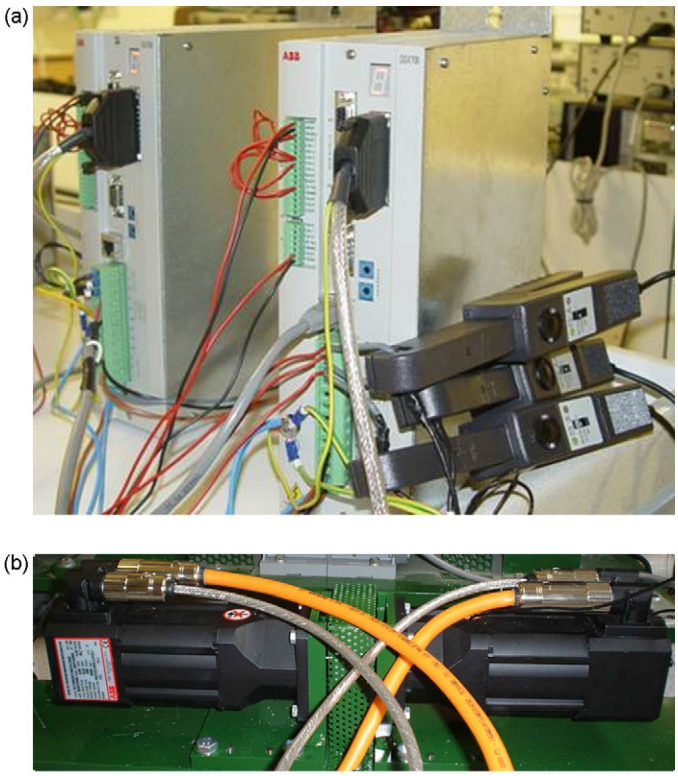

Fig. 1. (a) Voltage source inverters with the current probes. (b) PMSMs experimental rig.

4.1. Fast Fourier transform (FFT)

In this section FFT is used to carry out a preliminary study to detect the exact experimental harmonic frequencies for both healthy and faulty motors.

Firstly, the amplitude spectrum of a healthy and a partially demagnetized motor operating both at a constant speed of 6000 rpm ($f_e = 300$ Hz) and under rated load are obtained (Fig. 3).

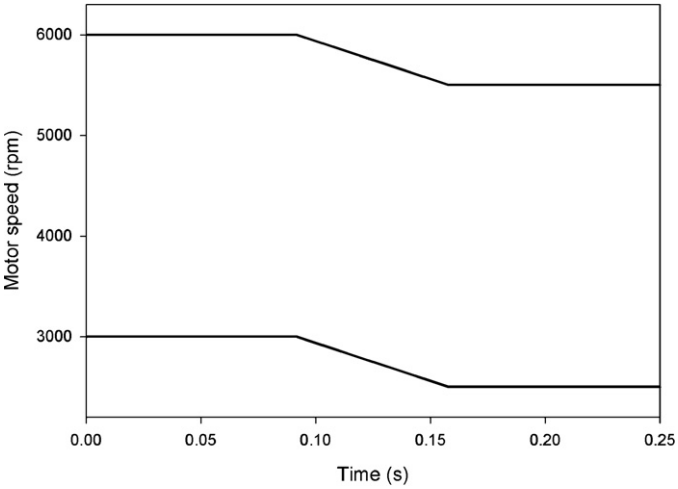

Fig. 2. Speed changes applied from 6000 to 5500 and 3000 to 2500 rpm.

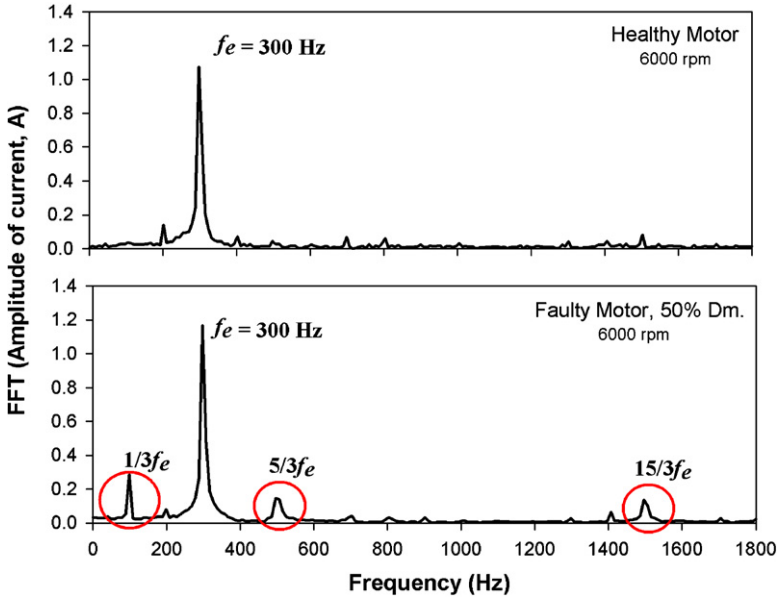

Fig. 3. FFT stator current spectrum for a constant speed of 6000 rpm operating at rated load.

Fig. 3 corroborates the predictions of Eq. (2). Whereas a healthy motor has a dominant harmonic placed in f_e, a partially demagnetized motor presents the main faulty harmonics placed in $f_e/3$, $5f_e/3$ and $15f_e/3$.

More complex is the interpretation of the FFT analysis of the stator currents when the PMSM runs under non-stationary speed conditions. Fig. 4 shows the resulting FFT spectrum of a healthy and a partially demagnetized motor under a speed change from 6000 to 5500 rpm operating at one-half full load (one-half rated load). As it is shown, FFT mixes frequency harmonics when the motor operates at variable speeds between 6000 and 5500 rpm.

However, without prior knowledge of the signal displayed in Fig. 4, it is impossible to diagnose if the harmonics related to 6000 and 5500 rpm appear at different times due a change of speed of the PMSM or if, on the contrary, they appear simultaneously for a determined speed of the PMSM. Thus, even though FFT is extremely useful when dealing with stationary signals, amplitude and frequency outputted by the FFT do not contain information about time, a serious drawback that can lead to an erroneous diagnostic. As stated in Ref. [21], the Fourier analysis has some restrictions; the system must be linear and the data must be strictly periodic or stationary. The Fourier transform of a non-stationary signal tends to average the frequency content of the signal over time. Therefore, FFT is not well suited to perform a correct diagnostic of the machine when dealing with non-stationary conditions.

4.2. Hilbert Huang transform (HHT)

As mentioned previously, FFT is not the best choice when dealing with non-stationary signals. For fault detection in PMSMs working in non-stationary conditions, we propose the Hilbert Huang transform.

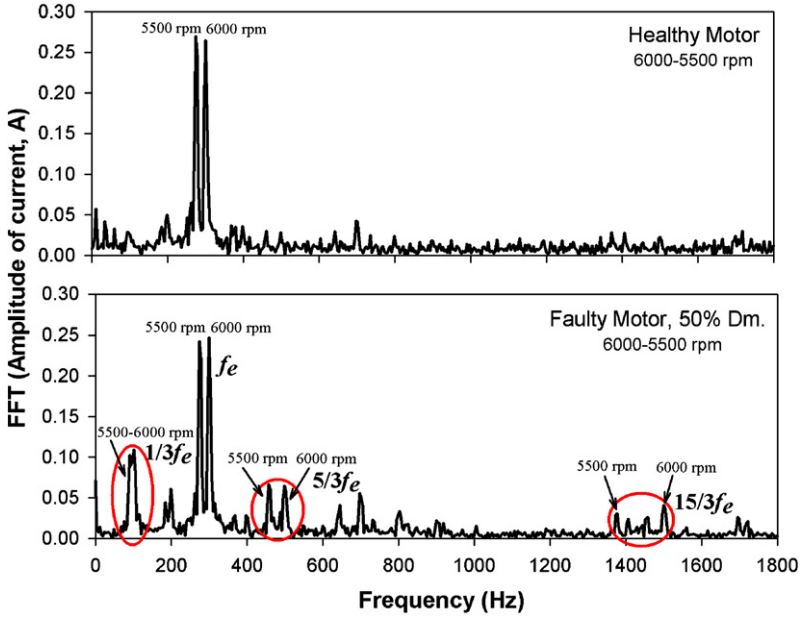

Fig. 4. FFT stator current spectrum for a speed change from 6000 to 5500 rpm operating at one-half rated load.

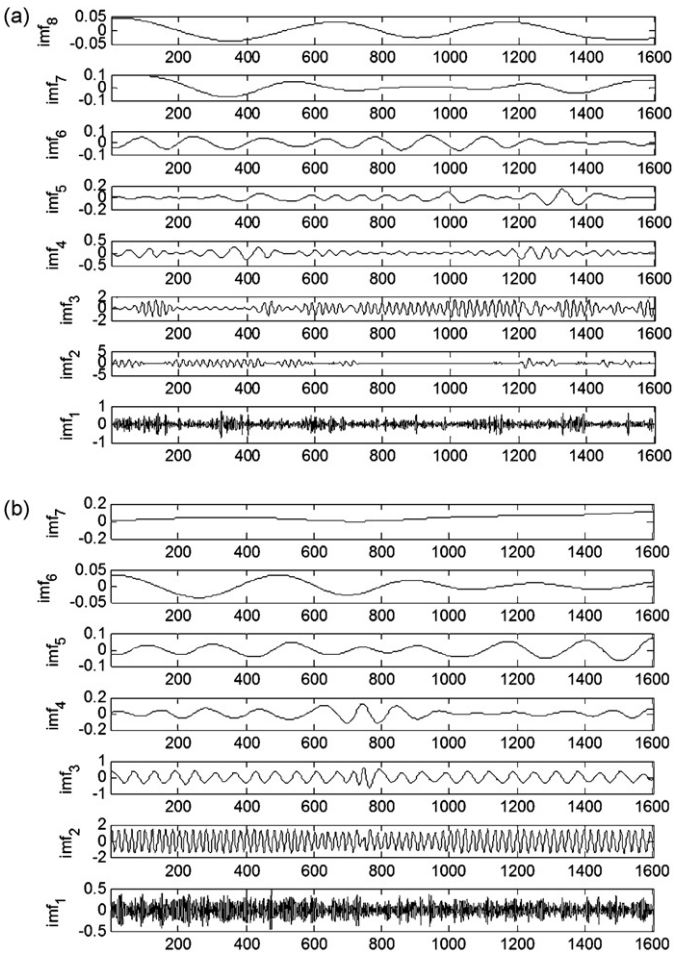

Fig. 5. Stator current EMD decomposition for a speed change from 6000 to 5500 rpm when the motor operates at rated load. (a) Healthy motor and (b) demagnetized motor.

Once the experimental signal has been acquired (in the case studied it is the stator current acquired at 6 kHz), the first step involved with the HHT is performing the empirical mode decomposition, from which the IMFs emerge. Fig. 5 shows the IMFs resulting from the stator current of a healthy motor under a speed change from 6000 to 5500 rpm operating at full load (rated current).

Although some authors use the information provided by the IMFs to compute a finite set of features that allows discrimination between both healthy and faulty states, the number of IMFs obtained from the EMD is not constant, as shown in Fig. 5. This means that different stator current acquisitions can lead to a different number of IMFs computed by the EMD algorithm. Therefore, we prefer to compute the discriminating features not directly from the IMFs, but from the Hilbert Huang time–frequency representation of the acquired stator current instead.

Once the EMD has been performed, the second step involved in the HHT is computing the Hilbert transform. This algorithm takes as inputs the IMFs obtained from the EMD and outputs a matrix containing the time–frequency representation of the original data, also called Hilbert Huang spectrum.

The Hilbert Huang spectrums for both a healthy and a partially demagnetized PMSM when running under a speed change from 6000 to 5500 rpm are shown in Figs. 6 and 7. In these plots, the horizontal axis represents time and the vertical axis is frequency. Additionally, a third dimension indicating the amplitude of a particular frequency at a particular time is represented by the intensity or color of each point in the image. The colorbar on the right-hand

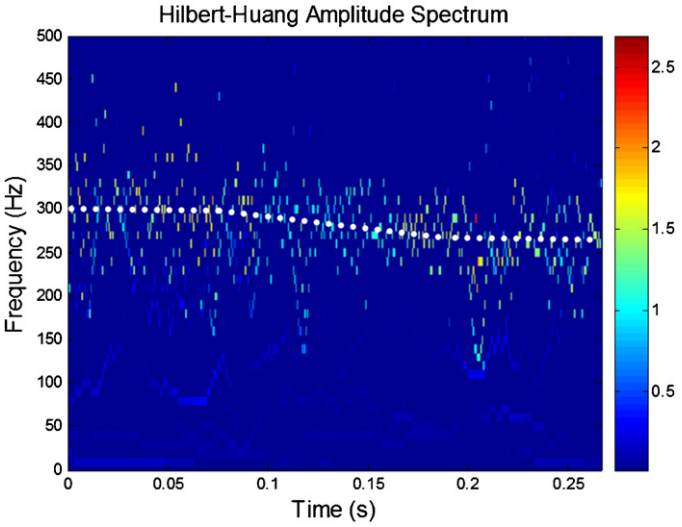

Fig. 6. Stator current time–frequency representation from the HHT output of a healthy PMSM for a speed change from 6000 to 5500 rpm operating at rated load.

side of the figure indicates the range of amplitudes displayed in the time–frequency HHT spectrum plot. The dotted white line superimposed in Figs. 6 and 7 shows the applied speed change.

The color of the points of Fig. 6 indicate the strength of the amplitude of the HHT spectrum at a given time–frequency point. Therefore, a dark blue point indicates that its value is close to 0, whereas a red point indicates that its value is close to 2.5.

The Hilbert Huang transform outputs a $r \times c$ matrix M, r being the number of rows (frequency samples) and c the number of columns (time samples). In the case analyzed in the present study we have imposed 300 rows (frequency samples) and 1601 columns (time samples). As the sampling frequency is 6 kHz, due to the Nyquist criterion, the rows of matrix M contain information between 0 and 3000 Hz. Thus, the frequency (row) resolution is approximately 10 Hz (300 rows from 0 to 3000 Hz) while the time (column) resolution is 1/6000 s. In order to visualize in detail the main frequencies of interest, Figs. 6 and 7 plot the information provided by the matrix M in the frequency band between 0 and 500 Hz.

It is evident that from Figs. 6 and 7 that it is difficult to discriminate between faulty and healthy conditions because the

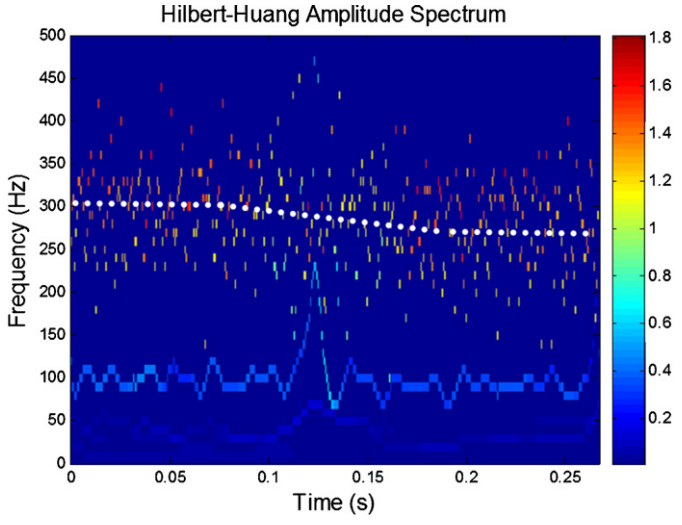

Fig. 7. Stator current time–frequency representation from the HHT output of a partially demagnetized PMSM for a speed change from 6000 to 5500 rpm operating at rated load.

Table 1
Relation between rows of the time–frequency matrix outputted by HHT and fault frequencies under the speed changes analyzed.

	Fault frequency (Hz)	Lower and upper rows	Lower and upper frequencies (Hz)
6000–5500 rpm (f_e: 300–275 Hz, FR = 10 Hz)			
E_{10} (f_e/3)	100–91.7	8–12	80–120
E_{30} (f_e)	300–275	24–36	240–360
E_{50} (5f_e/3)	500–458	40–60	400–600
E_{150} (15f_e/3)	1500–1375	120–180	1200–1800
3000–2500 rpm (f_e: 150–137.5 Hz, FR = 10 Hz)			
E_5 (f_e/3)	50–45.8	4–6	40–60
E_{15} (f_e)	150–137.5	12–18	120–180
E_{25} (5f_e/3)	250–229.2	20–30	200–300
E_{75} (15f_e/3)	750–687.5	60–90	600–900

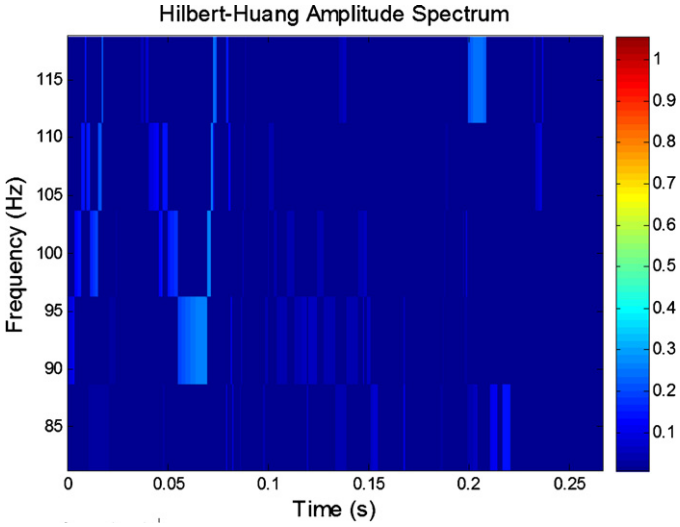

Fig. 8. Stator current time–frequency representation around f_e/3 of a healthy PMSM for a speed change from 6000 to 5500 rpm operating at rated load.

information contained in the time–frequency matrix M with dimensions 300 × 1601 is too vast for practical applications. Thus, a feature extraction method capable of condensing the essential information in a finite set of appropriate features is desirable.

In this paper the use of a reduced set of features to discriminate between a healthy and a faulty motor is proposed. These features

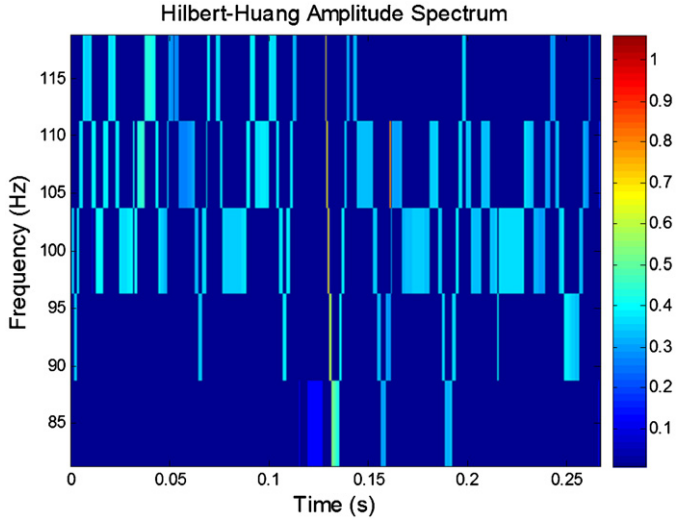

Fig. 9. Stator current time–frequency representation around f_e/3 of a partially demagnetized PMSM for a speed change from 6000 to 5500 rpm operating at rated load.

are selected in order to provide information about the faulty harmonic frequencies underlying in the original signal. The first step is to identify the rows of the time–frequency matrix M containing the faulty frequencies. Selection of a security or tolerance interval around each faulty frequency of interest is also suggested in order to account for possible experimental errors of the measured speed as well as potential uncertainties due to the data processing method.

The criterion shown in Eq. (18) for selecting the rows of the HHT output matrix M according to the harmonic frequencies to be detected is proposed.

$$[r\_min, r\_max] = [0.8FR^{-1}f_{fault},\ \ 1.2FR^{-1}f_{fault}] \tag{18}$$

f_{fault} being the fault frequency to be detected, r is the row position in matrix M and FR is its frequency resolution. In the case studied FR = 10 Hz. Factors 0.8 and 1.2 are the tolerance of the interval of frequencies analyzed around the fault frequency of interest which can be modified.

Next, the percentage of energy contained in each interval is computed as explained in Eq. (19).

$$E_z = 100 \times \frac{\sum_{i=r\_min\,i}^{r\_max}\sum_{j=1}^{c} M_{i,j}^2}{\sum_{i=1}^{r}\sum_{j=1}^{c} M_{i,j}^2} \tag{19}$$

c and r being, respectively, the total number of columns and rows of the time–frequency matrix M, [r_min,r_max] the interval of rows to be considered and z the central row of the selected interval.

The objective of the energy-related features computed in this work is to reduce the amount of data arising from the HHT, simplifying notably the data structure of the problem – it allows reducing the computational burden of the problem in the diagnosis stage – while retaining as much as possible of the relevant information contained in the data outputted by the HHT. Although under this approach the information of each frequency band is reduced to a

Table 2
Energy in percentage for the 4 computed energy-related features (mean value of I_a, I_b and I_c) computed from the HHT output matrix M.

Motor	E_{10}	E_{30}	E_{50}	E_{150}
6000–5500 rpm, full load				
Healthy	1.83	87.39	9.61	1.17
50% Dm	7.43	77.25	13.97	1.35
6000–5500 rpm, one-half load				
Healthy	5.57	77.72	12.61	4.10
50% Dm	16.72	62.94	16.66	3.68
Motor	E_5	E_{15}	E_{25}	E_{75}
3000–2500 rpm, full load				
Healthy	2.71	83.96	12.15	1.17
50% Dm	4.24	80.28	14.91	0.58
3000–2500 rpm, one-half load				
Healthy	4.19	78.39	12.37	5.06
50% Dm	11.06	69.94	17.42	1.58

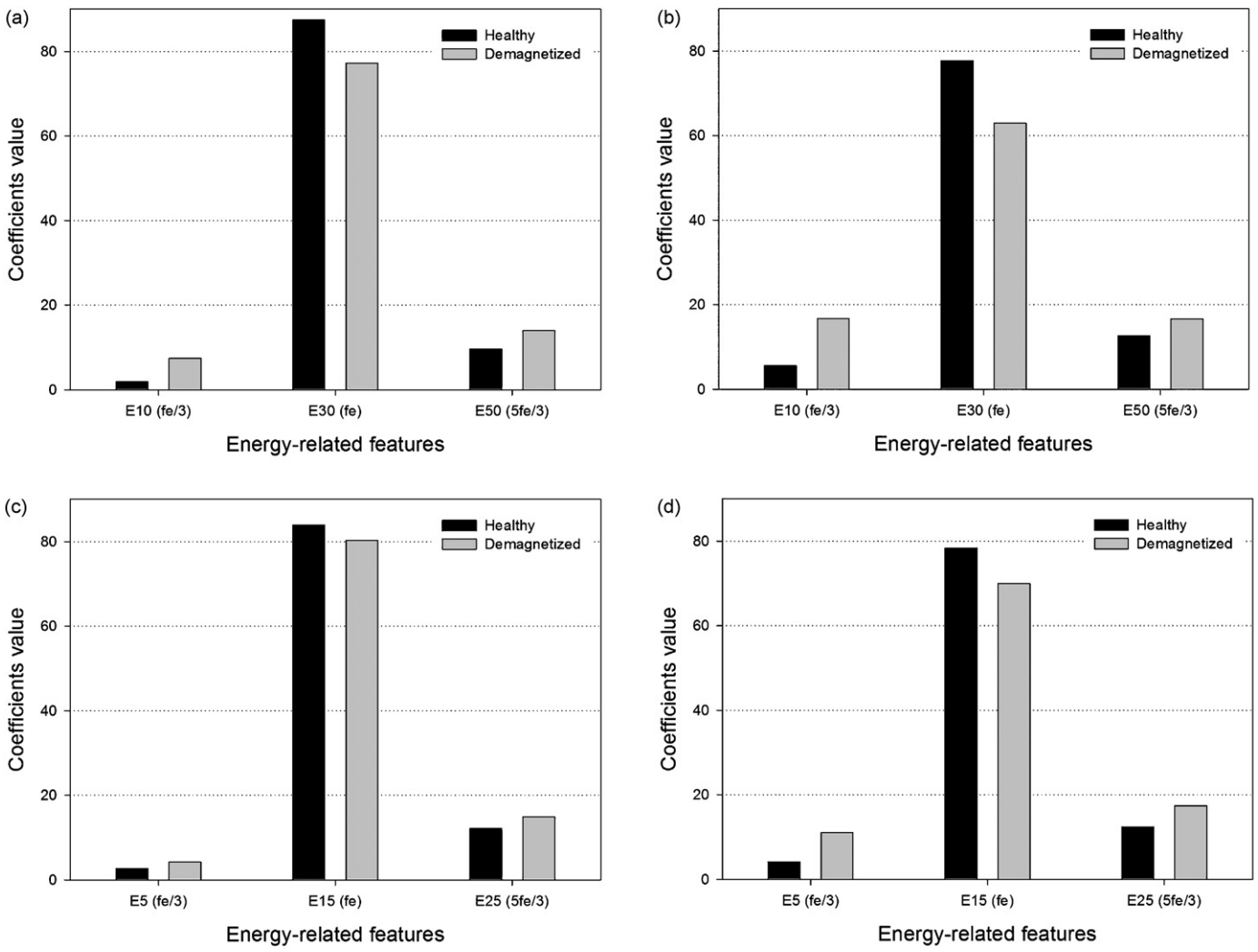

Fig. 10. Values of the energy-related features. (a) Speed change from 6000 to 5500 rpm and full load, (b) speed change from 6000 to 5500 rpm and one-half load, (c) speed change from 3000 to 2500 rpm and rated load and (d) speed change from 3000 to 2500 rpm and one-half rated load.

single value, this value is obtained from the integral over the whole time domain of the square of the amplitudes arising from the HHT. Thus, this single value has been obtained from the "average" of the square of the amplitudes arising from the HHT over the whole time-domain interval. This procedure is necessary to generate a system fast enough to carry out an automatic on-line diagnostic in industrial applications.

Table 1 summarizes the rows chosen to compute the features E_z selected for the problem under study.

Figs. 8 and 9 show, respectively, the time–frequency representation of rows 8–12 (corresponding at faulty frequency $f_e/3$) of the stator current of a healthy and a partially demagnetized motor under a speed change from 6000 to 5500 rpm when operating at rated load.

As depicted in Figs. 8 and 9, the energy content around the faulty harmonic $f_e/3$ is much higher when dealing with a partially demagnetized PMSM compared to a healthy one. Essential information provided by Figs. 8 and 9 is condensed in coefficient E_{10}, which is more useful for diagnosis purposes than the above mentioned figures.

Table 2 summarizes the information provided by the 4 computed energy-related features. It clearly shows that some of these features allow discrimination between a healthy and a partially demagnetized motor condition.

Fig. 10 shows the results of Table 2 in graph form.

It is important to highlight that fault harmonic frequencies change with rotor speed. Thus, under non-stationary conditions, information provided by the proposed features may change regarding rotor speed. Fortunately, the speed controller which drives the PMSM provides the actual speed of the machine. Thus, a simple algorithm can compute Eq. (18) and adjust automatically the row intervals of the time–frequency matrix M from which the set of features is calculated. Thus, the method proposed in this work allows fault detection for different speeds and load conditions.

5. Conclusion

In this paper the effect of demagnetization faults that are reflected on the stator current spectrum of a PMSM has been analyzed by applying a time–frequency approach.

Results of FFT of acquired stator currents for a PMSM driven by a vector control have indicated that faulty harmonics are visible in the current spectrum. However, fault detection by means of FFT is not clear when the PMSM runs under non-stationary speed conditions. Although FFT allows detecting demagnetization faults by analyzing the amplitude of harmonics in stationary signals, it is not the best choice to detect motor failures when dealing with non-stationary signals.

In order to detect faults in motors running under non-stationary conditions, time–frequency processing methods are proposed.

Specifically, a HHT-based method has been successfully applied in this paper to discriminate between healthy and partially demagnetized PMSM running under non-stationary speed conditions.

The proposed HHT-based method computes a reduced set of discriminating features that are specific for each fault frequency harmonic of the stator currents. Thus, this method is well suited to detect possible motor failures for on-line diagnostic systems in industrial applications when the motor is running under non-stationary conditions.

Fault harmonic frequencies change when the motor operates under dynamic conditions. Information provided by the proposed features also changes relative to rotor speed. Fortunately, the speed controller that drives the PMSM provides the actual speed of the machine. Thus, a simple algorithm can be computed that automatically adjusts the interval of data from which feature extraction is made. Consequently, the method proposed in this work allows fault detection regardless of the speed or load conditions.

References

[1] S. Rajagopalan, W. le Roux, T.G. Habetler, R.G. Harley, Dynamic eccentricity and demagnetized rotor magnet detection in trapezoidal flux (brushless DC) motors operating under different load conditions, IEEE Trans. Power Electron. 22 (2007) 2061–2069.

[2] M. Dai, A. Keyhani, T. Sebastian, Fault analysis of a PM brushless DC motor using finite element method, IEEE Trans. Energy Conv. 20 (2005) 1–6.

[3] H. Razika, H. Henao, R. Carlson, An induction machine model including interbar currents for studying, Electr. Power Syst. Res. 79 (2009) 181–189.

[4] H. Calıs, A. Cakır, Rotor bar fault diagnosis in three phase induction motors by monitoring fluctuations of motor current zero crossing instants performances during transients and steady state, Electr. Power Syst. Res. 77 (2007) 385–392.

[5] Z. Ye, A. Sadeghian, B. Wu, Mechanical fault diagnostics for induction motor with variable speed drives using Adaptive Neuro-fuzzy Inference System, Electr. Power Syst. Res. 76 (2006) 742–752.

[6] K. Bacha, H. Henao, M. Gossa, G.A. Capolino, Induction machine fault detection using stray flux EMF measurement and neural network-based decision, Electr. Power Syst. Res. 78 (2008) 1247–1255.

[7] R. Samsi, A. Ray, J. Mayer, Early detection of stator voltage imbalance in three-phase induction motors, Electr. Power Syst. Res. 79 (2009) 239–245.

[8] Y. Gritli, Y.A. Stefani, A. Chatti, C. Rossi, F. Filippetti, The combined use of the instantaneous fault frequency evolution and frequency sliding for advanced rotor fault diagnosis in DFIM under time-varying condition, in: Proc. IEEE Industrial Electronics Conference, IECON'09, November, 2009, pp. 3471–3476.

[9] F. Morel, X. Lin-Shi, J.M. Rétif, B. Allard, A predictive current control applied to a permanent magnet synchronous machine, comparison with a classical direct torque control, Electr. Power Syst. Res. 78 (2008) 1437–1447.

[10] Y. Ait-gougam, R. Ibtiouen, O. Touhami, J.-P. Louis, M. Gabsi, Inverse modelling and pulsating torque minimization of salient pole sinusoidal synchronous machines, Electr. Power Syst. Res. 78 (2008) 88–96.

[11] R.M. Jan, C.S. Tseng, R.J. Liu, Robust PID control design for permanent magnet synchronous motor: a genetic approach, Electr. Power Syst. Res. 78 (2008) 1161–1168.

[12] W. le Roux, R.G. Harley, T.G. Habetler, Detecting rotor faults in low power permanent magnet synchronous machines, IEEE Trans Power Electron 22 (2007) 322–328.

[13] W. le Roux, R.G. Harley, T.G. Habetler, Detecting faults in rotors of PM drives, IEEE Ind. Appl. Mag. 14 (2008) 23–31.

[14] S. Rajagopalan, Detection of rotor and load faults in brushless dc motors operating under stationary and nonstationary conditions, PhD Thesis, Georgia Institute of Technology, August 2006.

[15] W. le Roux, R.G. Harley, T.G. Habetler, Detecting rotor faults in low power permanent magnet synchronous machines, IEEE Trans. Power Electron. 22 (2007) 322–328.

[16] D. Casadei, F. Filippetti, C. Rossi, A. Stefani, Magnets faults characterization for permanent magnet synchronous motors, in: Proc. IEEE International Symposium on Diagnostics for Electric Machines, Power Electronics and Drives, SDEMPED'09, August, 2009, pp. 1–6.

[17] A. Roy, C.H. Wen, J.F. Doherty, J.D. Mathews, Signal feature extraction from microbarograph observations using the Hilbert-Huang transform, IEEE Trans. Geosci. Remote Sens. 46 (2008) 1442–1447.

[18] J. Antonino-Daviu, M. Riera-Guasp, J. Roger-Folch, F. Martínez-Giménez, A. Peris, Application and optimization of the discrete wavelet transform for the detection of broken rotor bars in induction machines, Appl. Comput. Harmon. Anal. 21 (2006) 268–279.

[19] S.G. Mallat, A Wavelet Tour of Signal Processing, Academic Press, San Diego, 1998.

[20] J.A. Antonino-Daviu, M. Riera-Guasp, J. Roger-Folch, R.B. Perez, An analytical comparison between DWT and Hilbert-Huang-based methods for the diagnosis of rotor asymmetries in induction machines, in: Conference Record of the Industry Applications Conference, 42nd IEEE-IAS Annual Meeting, vol. 1, 2007, pp. 1932–1939.

[21] N.E. Huang, Z. Shen, S.R. Long, M.C. Wu, H.H. Shih, Q. Zheng, N.C. Yen, C.C. Tung, H.H. Liu, The empirical mode decomposition and the Hilbert spectrum for nonlinear and non-stationary time series analysis, Proc. R. Soc. Lond. A 454 (1998) 903–995.

[22] G. Kerschen, A.F. Vakakis, Y.S. Lee, et al., Toward a fundamental understanding of the Hilbert-Huang transform in nonlinear structural dynamics, J. Vib. Control 14 (2008) 77–105.

[23] A.D. Veltcheva, C.G. Soares, Analysis of abnormal wave records by the Hilbert-Huang transform method, J. Atmos. Ocean Technol. 24 (2007) 1678–1689.

[24] X. Li, D. Li, Z. Liang, L.J. Voss, J.W. Sleigh, Analysis of depth of anesthesia with Hilbert-Huang spectral entropy, Clin. Neurophysiol. 119 (2008) 2465–2475.

[25] D.J. Yu, Y. Yang, J.S. Cheng, Application of time–frequency entropy method based on Hilbert-Huang transform to gear fault diagnosis, Measurement 40 (2007) 823–830.

[26] M.A. Andrade, A.R. Messina, C.A. Rivera, D. Olguin, Identification of instantaneous attributes of torsional shaft signals using the Hilbert transform, IEEE Trans. Power Syst. 19 (2004) 1422–1429.

[27] N. Senroy, Generator coherency using the Hilbert-Huang transform, IEEE Trans. Power Syst. 23 (2008) 1701–1708.

[28] B. Lu, B.R. Upadhyaya, R.B. Perez, Structural integrity monitoring of steam generator tubing using transient acoustic signal analysis, IEEE Trans. Nuclear Sci. 52 (2005) 484–493.

[29] R. Yan, R.X. Gao, A tour of the tour of the Hilbert-Huang transform: an empirical tool for signal analysis, IEEE Instrum. Meas. Mag. 10 (2007) 40–45.

[30] G. Rilling, P. Flandrin, P. Gonçalves, On empirical mode decomposition and its algorithms, in: IEEE-EURASIP Workshop on Nonlinear Signal and Image Processing NSIP-03, Grado, Italy, June, 2003.

[31] R. Yan, R.X. Gao, Hilbert-Huang transform-based vibration signal analysis for machine health monitoring, IEEE Trans. Instrum. Meas. 55 (2006) 2320–2329.

[32] E.B. Saff, A.D. Snider, Complex Analysis for Mathematics, Science and Engineering, Prentice-Hall Inc., New York, 1976.

[33] H. Peter, Applied and Computational Complex Analysis, vol. 1, John Wiley & Sons Inc., New York, 1988.

[34] G. Rilling, Empirical Mode Decomposition, http://perso.ens-lyon.fr/patrick.flandrin/emd.html.